nature photonics

Article

https://doi.org/10.1038/s41566-022-01077-w

Observation of the quantum Gouy phase

In the format provided by the authors and unedited

Supplementary material to: Observation of the quantum Gouy phase

Markus Hiekkamäki[1*], Rafael F. Barros[1], Marco Ornigotti[1] and Robert Fickler[1]

[1]Photonics Laboratory, Physics Unit, Tampere University, Tampere, FI-33720, Finland.

1 Derivation of the quantum Gouy phase

The quantum Gouy phase is the phase acquired by a Fock state of a paraxial mode upon propagation. To derive this phase, let us consider the transformation of the mode corresponding to the operator [1, 2]

$$\hat{a}^\dagger_{\ell p}(0) = \int\int u_{\ell p}(\boldsymbol{\rho}, 0)\hat{a}^\dagger(\boldsymbol{\rho})d^2\rho\,, \tag{S1}$$

upon a translation of z along the optical axis

$$\hat{a}^\dagger_{\ell p}(z) = e^{-\mathrm{i}\hat{P}_z z/\hbar}\hat{a}^\dagger_{\ell p}(0)e^{\mathrm{i}\hat{P}_z z/\hbar}\,, \tag{S2}$$

where $\hat{a}^\dagger_{\ell p}(z)$ represents the transverse mode at any plane z characterized by the integers ℓ and p, $\boldsymbol{\rho}$ contains the transverse coordinates, $\hat{a}^\dagger(\boldsymbol{\rho})$ is an operator density, and $u_{\ell p}(\boldsymbol{\rho}, 0)$ is the normalized structure of the mode. The operator $\hat{P}_z$ is the longitudinal component of the linear momentum operator, defined for a monochromatic field in the plane wave basis as

$$\hat{P}_z = \int\int \hbar k_z(\boldsymbol{\kappa}_j)\hat{a}^\dagger(\boldsymbol{\kappa}_j)\hat{a}(\boldsymbol{\kappa}_j)d^2\kappa_j\,, \tag{S3}$$

where $k_z(\boldsymbol{\kappa}_j)$ is the longitudinal wave vector for the mode j, which depends on the transverse wave vector $\boldsymbol{\kappa}_j$ as $k_z(\boldsymbol{\kappa}_j) = \sqrt{k^2 - \|\boldsymbol{\kappa}_j\|^2}$, with k being the wave number, common to all of the plane wave modes $\hat{a}^\dagger(\boldsymbol{\kappa}_j)$. To operate on our mode with this unitary, we initially express our mode in the plane wave basis as

$$\hat{a}^{\dagger}_{\ell p}(0) = \int\int F_{\ell p}(\boldsymbol{\kappa}, 0)\hat{a}^{\dagger}(\boldsymbol{\kappa})d^2\kappa\,, \tag{S4}$$

where $F_{\ell p}(\boldsymbol{\kappa}, 0)$ is the normalized angular spectrum of the mode ℓp at $z = 0$. Now we can restate Eq. (S2)

$$\hat{a}^{\dagger}_{\ell p}(z) = \int\int F_{\ell p}(\boldsymbol{\kappa}, 0)e^{-\mathrm{i}\hat{P}_z z/\hbar}\hat{a}^{\dagger}(\boldsymbol{\kappa})e^{\mathrm{i}\hat{P}_z z/\hbar}d^2\kappa, \tag{S5}$$

then using the Baker-Hausdorff lemma, we can finally obtain

$$\hat{a}^{\dagger}_{\ell p}(z) = \int\int F_{\ell p}(\boldsymbol{\kappa}, 0)e^{-\mathrm{i}k_z(\boldsymbol{\kappa})z}\hat{a}^{\dagger}(\boldsymbol{\kappa})d^2\kappa. \tag{S6}$$

The form of Eq. (S6) is now identical to a mode with an angular spectrum $F_{\ell p}(\boldsymbol{\kappa}, 0)$ propagated by a distance z using the angular spectrum method (ASM) [3, 4]. Since the ASM accounts for every aspect of paraxial beam propagation, including the Gouy phase and the plane wave phase $e^{-\mathrm{i}kz}$, we can extract the Gouy phase out of the translated mode by initially expressing the translated mode in real space using the complex field distribution

$$\begin{aligned}\hat{a}^{\dagger}_{\ell p}(z) &= \int\int F_{\ell p}(\boldsymbol{\kappa}, 0)e^{-\mathrm{i}k_z(\boldsymbol{\kappa})z}\hat{a}^{\dagger}(\boldsymbol{\kappa})d^2\kappa \\ &= e^{-\mathrm{i}kz}\int\int u_{\ell p}(\boldsymbol{\rho}, z)\hat{a}^{\dagger}(\boldsymbol{\rho})d^2\rho\,,\end{aligned} \tag{S7}$$

where $u_{\ell p}(\boldsymbol{\rho}, z)$ is the normalized transverse field for the mode, calculated classically through the ASM. We can then choose an artificial set of orthogonal spatial modes $\hat{b}^{\dagger}_{\ell p}(z)$ which have exactly the structure of the ℓp modes at the position z, without the Gouy phase, i.e., $u'_{\ell p}(\boldsymbol{\rho}, z) = u_{\ell p}(\boldsymbol{\rho}, z)e^{-\mathrm{i}kz}e^{\mathrm{i}\Phi_G}$. Expressing the position basis mode density in this new mode basis $\hat{a}^{\dagger}(\boldsymbol{\rho}) = \sum_{\ell' p'} u'^{*}_{\ell' p'}(\boldsymbol{\rho}, z)\hat{b}^{\dagger}_{\ell' p'}(z)$ the translated mode takes the form

$$\hat{a}^{\dagger}_{\ell p}(z) = \sum_{\ell' p'} e^{-\mathrm{i}\Phi_G}\hat{b}^{\dagger}_{\ell' p'}(z)\int\int u^{*}_{\ell' p'}(\boldsymbol{\rho}, z)u_{\ell p}(\boldsymbol{\rho}, z)\,d^2\rho\,. \tag{S8}$$

Due to the orthonormality of the chosen spatial mode basis [5], the above integral reduces to

$$\hat{a}^{\dagger}_{\ell p}(z) = \sum_{\ell' p'} \delta_{\ell' \ell}\delta_{p' p}e^{-\mathrm{i}\Phi_G}\hat{b}^{\dagger}_{\ell' p'}(z) = e^{-\mathrm{i}\Phi_G}\hat{b}^{\dagger}_{\ell p}(z)\,. \tag{S9}$$

Hence, we can then state the evolution of an N-photon Fock state in the spatial mode ℓp as

$$\begin{aligned}|N\rangle_{\ell p;\,0} = \frac{\left(\hat{a}^{\dagger}_{\ell p}(0)\right)^N}{\sqrt{N!}}|0\rangle \rightarrow &\frac{\left(\hat{b}^{\dagger}_{\ell p}(z)e^{-\mathrm{i}(kz+\Phi_G)}\right)^N}{\sqrt{N!}}|0\rangle \\ &= e^{-\mathrm{i}Nkz-\mathrm{i}N\Phi_G}\,|N\rangle_{\ell p;\,z}\,,\end{aligned} \tag{S10}$$

showing that upon translation, any phase accumulated by the mode results in N-times the same phase being accumulated by the N-photon Fock state.

Interestingly, from the fact that any arbitrary mode $\hat{b}(z)$ can be chosen, one can infer that any changes in the amplitude of the field during propagation is also magnified N-times. Similarly to the N-times increase in the phase however, in order to observe this N-fold change in the amplitude the measurement needs to be chosen in a manner that displays this change. One example of such a measurement is the post-selection on both of the photons existing in the same spatial position which manifests as an increased confinement in Fig. 1c) of the main text. Similarly, the same can be seen in the measured data in Fig. 3 as a narrowing of the envelope within which the fringes are observed. As a result, these changes could be summarized as the state experiencing any change in the mode to the power of N, which is in conflict with the effective de Broglie wavelength interpretation whenever the amplitude changes or a phase is acquired that has a nonlinear dependence on the wavenumber.

2 Derivation of the measurement probability

To model the expected measurement signal we calculate the probability of N photons coupling into a single mode fiber (SMF) from a radial mode N00N state. We start off with the radial mode N00N state at position z

$$|\Psi(z)\rangle = \frac{1}{\sqrt{2}}\left(|N\rangle_{0p;\,z}\,|0\rangle_{0p';\,z} - e^{\mathrm{i}\theta}\,|0\rangle_{0p;\,z}\,|N\rangle_{0p';\,z}\right), \tag{S11}$$

where θ is a constant phase offset between the two terms. By decomposing the eigenmode of the SMF into a superposition of LG modes at a distance z from the beam waist

$$\hat{a}_f^\dagger = A_p(z)\hat{a}_{0p}^\dagger(z) + A_{p'}(z)\hat{a}_{0p'}^\dagger(z) + \cdots + A_{nq}(z)\hat{a}_{nq}^\dagger(z) + \ldots, \tag{S12}$$

we can calculate the probability of N photons coupling into the SMF using

$$\begin{aligned} P =& \frac{1}{N!}|\langle\Psi(z)|\hat{a}_f^{\dagger N}|0\rangle|^2 \\ =& \frac{1}{2N!}\Big|\left(\langle N|_{0p;\,z}\,\langle 0|_{0p';\,z} - e^{-\mathrm{i}\theta}\,\langle 0|_{0p;\,z}\,\langle N|_{0p';\,z}\right) \\ & \left(A_p(z)\hat{a}_{0p}^\dagger(z) + A_{p'}(z)\hat{a}_{0p'}^\dagger(z) + \ldots\right)^N|0\rangle\Big|^2. \end{aligned} \tag{S13}$$

Note that in the above equations, using the normalized transverse structures, the overlaps are defined as

$$A_{\ell p}(z) = \int\int u_{\ell p}^*(\boldsymbol{\rho}, z)\, u_{\mathrm{SMF}}(\boldsymbol{\rho})\, d^2\rho\,, \tag{S14}$$

which also includes the Gouy phase of each mode (note that for $A_p(z)$, $\ell = 0$). From the overlap calculation in Eq. (S13), only the states with N photons in either mode $0p$ or $0p'$ survive and the above equation simplifies to

$$
\begin{aligned}
P =& \frac{1}{2}\Big| \left(\langle N|_{0p;\,z} - e^{-\mathrm{i}\theta} \langle N|_{0p';\,z} \right) \\
& \left(A_p^N(z) \, |N\rangle_{0p;\,z} + A_{p'}^N(z) \, |N\rangle_{0p';\,z} \right) \Big|^2 \\
=& \frac{1}{2} \left| A_p^N(z) - e^{-\mathrm{i}\theta} A_{p'}^N(z) \right|^2 .
\end{aligned}
\tag{S15}
$$

To get a more intuitive expression of this equation, we can further state $A_i(z) = e^{\mathrm{i}(\Phi_G(z)+\phi(z))}|A_i(z)|$, where $\phi(z)$ is small since the SMF only probes the phase difference close to the optical axis where the phase of the overlap is mostly dependent on the Gouy phase and not the changing wavefront curvature. By then defining the Gouy phase difference as $\Delta\Phi_G(z) = \Phi'_G - \Phi_G$ (Φ_G and Φ'_G correspond to Gouy phases acquired by LG modes of different mode order $S = 2p + 1$ and $S' = 2p' + 1$) we can write the probability as

$$
\begin{aligned}
P =& \frac{1}{2} \left| |A_p(z)|^N - e^{\mathrm{i}(N\Delta\Phi_G(z) - \theta + N\phi(z))} |A_{p'}(z)|^N \right|^2 \\
=& \frac{1}{2} \Big[|A_p(z)|^{2N} + |A_{p'}(z)|^{2N} \\
& - 2|A_p(z)|^N |A_{p'}(z)|^N \cos(N\Delta\Phi_G(z) - \theta + N\phi(z)) \Big] .
\end{aligned}
\tag{S16}
$$

From the form of this equation, it is clear that the probability amplitude oscillates according to $\cos(2N(p' - p) \times \mathrm{atan}(z/z_R))$, meaning that the oscillations get less frequent the further away we go from $z = 0$. In addition to this, the oscillation happens inside an envelope function defined by the overlaps $|A_p|$ and $|A_{p'}|$.

To derive a similar expected signal for the case of a classical monochromatic field with the normalized transverse structure $u_{\mathrm{total}}(\boldsymbol{\rho}, z) = \frac{1}{\sqrt{2}}(u_{0p}(\boldsymbol{\rho}, z) - e^{\mathrm{i}\theta} u_{0p'}(\boldsymbol{\rho}, z))$ being coupled into the SMF, we can calculate the power of the light in the SMF as an overlap between the structure of the incident field and the normalized eigenmode of the SMF

$$
\begin{aligned}
P_L &\propto \left| \int\int \left(u_{0p}(\boldsymbol{\rho}, z) - e^{\mathrm{i}\theta} u_{0p'}(\boldsymbol{\rho}, z) \right)^* u_{SMF}(\boldsymbol{\rho}) d^2\rho \right|^2 \\
&= \left| \int\int u^*_{0p}(\boldsymbol{\rho}, z) u_{SMF}(\boldsymbol{\rho}) d^2\rho - e^{-\mathrm{i}\theta} \int\int u^*_{0p'}(\boldsymbol{\rho}, z) u_{SMF}(\boldsymbol{\rho}) \right|^2 \\
&= \left| A_p(z) - e^{-i\theta} A_{p'}(z) \right|^2 \\
&= \left[|A_p|^2 + |A_{p'}|^2 - 2|A_p||A_{p'}| \cos(\Delta\Phi_G - \theta + \phi(z)) \right] ,
\end{aligned}
\tag{S17}
$$

where the overlaps $A_i(z)$ correspond to the same overlaps calculated in Eq. (S14) and the same assumptions can be made about the overlaps near the optical axis.

3 Overlap between the eigenmode of a fiber and a Laguerre-Gaussian mode

To speed up the data processing, we analytically derived the overlap of a monochromatic p-mode and a Gaussian mode corresponding to the eigenmode of the SMF

$$A_p(z) = \int\int u^*_{0p}(\boldsymbol{\rho}, z) u_{\mathrm{SMF}}(\boldsymbol{\rho}) d^2\rho \,, \tag{S18}$$

where the normalized p-mode is defined according to [6]

$$\begin{aligned} u_{0p}(r,\varphi,z) =& \sqrt{\frac{2}{\pi}} \frac{1}{w(z)} \exp\left(-\frac{r^2}{w^2(z)}\right) L_p\left(\frac{2r^2}{w^2(z)}\right) \\ & \exp\left(\mathrm{i}\left[\frac{r^2 k}{2R} - (2p+1)\arctan\left(\frac{z}{z_R}\right)\right]\right) , \end{aligned} \tag{S19}$$

where r is the radial coordinate, φ is the azimuthal coordinate, $w(z) = w_0\sqrt{1+[(z-z_0)/z_R]^2}$ is the beam radius, $L_n(x) = \sum_{j=0}^{n} \binom{n}{j} \frac{(-1)^j}{j!} x^j$ is the Laguerre polynomial, w_0 is the beam waist, $R = z\left(1+[z_R/(z-z_0)]^2\right)$ is the curvature radius, $z_R = \frac{k w_0^2}{2}$ is the Rayleigh length, and k is the wave number. The normalized eigenmode of the fiber can be similarly defined as

$$u_{SMF}(r,\varphi) = \sqrt{\frac{2}{\pi}} \frac{1}{w_f} \exp\left(-\frac{r^2}{w_f^2}\right) . \tag{S20}$$

For simplicity we have set $z_0 = 0$ and insert the above definitions into equation (S18)

$$\begin{aligned} A_p(z) =& \frac{2}{\pi} \frac{1}{w_f w(z)} \exp\left(\mathrm{i}(2p+1)\arctan\left[\frac{z}{z_R}\right]\right) \times \\ & \int_0^\infty \int_0^{2\pi} r \exp\left(-r^2\left[\frac{1}{w_f^2} + \frac{1}{w^2(z)} + \mathrm{i}\frac{k}{2R}\right]\right) \times \\ & \sum_{j=0}^{p} \binom{p}{j} \frac{(-1)^j}{j!} \left(\frac{2r^2}{w^2(z)}\right)^j d\varphi dr \,. \end{aligned}$$

If we then define $B(z) = \frac{w(z)}{w_f} \exp\left(\mathrm{i}(2p+1)\arctan\left[\frac{z}{z_R}\right]\right)$, $C(z) = \frac{w^2(z)}{2}\left(\frac{1}{w_f^2} + \frac{1}{w^2(z)} + \mathrm{i}\frac{k}{2R(z)}\right)$, and $x(z) = \frac{2r^2}{w^2(z)}$, we can simplify the above equation to

$$A_p(z) = B(z) \int_0^\infty \exp\left[-C(z)x\right] \sum_{j=0}^{p} \binom{p}{j} \frac{(-1)^j}{j!} x^j dx \,. \tag{S21}$$

We can then use the identity $\int_0^\infty y^n \exp\left[-ay\right] dy = \frac{n!}{a^{n+1}}$, which holds when $Re(a) > 0$ and $n \in \mathbb{N}$, to arrive at the expression

$$A_p(z) = B(z)\left[\sum_{j=0}^{p}\binom{p}{j}\frac{(-1)^j}{C^{j+1}(z)]}\right], \tag{S22}$$

which we then used for calculating the overlaps in equations (S16) and (S17).

4 Derivation of the quantum Fisher information

The quantum Fisher information (QFI) carried by a probe state $|\psi(x)\rangle$ about a parameter x, encoded in the state by the unitary evolution $\hat{U}(x)$ is given by [7–9]

$$F_Q(|\psi(x)\rangle) = 4\Delta^2\hat{H}\,, \qquad \hat{H} = i\frac{d\hat{U}^\dagger(x)}{dx}\hat{U}(x)\,, \tag{S23}$$

where $\hat{H}$ is the generator of the unitary $\hat{U}$ and its variance $\Delta^2\hat{H} = \langle\hat{H}^2\rangle_\psi - \langle\hat{H}\rangle_\psi^2$ is taken with respect to the input state. In our case, where z is the longitudinal displacement, the translation operator $\hat{U} = e^{i\hat{P}_z z/\hbar}$ is the unitary of interest, yielding

$$F_Q(|\Psi(z)\rangle) = 4\frac{\Delta^2\hat{P}_z\big|_\Psi}{\hbar^2}\,. \tag{S24}$$

Thus, to obtain the QFI we need an expression for the variance of the longitudinal momentum operator, which we provide here for the radial N00N state (S11).

We start by using equations (S3) and (S11) to obtain

$$\begin{aligned}\langle\Psi(z)|\hat{P}_z|\Psi(z)\rangle &= \hbar\int\int k_z(\boldsymbol{\kappa})\,\langle\Psi(z)|\hat{a}^\dagger(\boldsymbol{\kappa})\hat{a}(\boldsymbol{\kappa})|\Psi(z)\rangle d^2\boldsymbol{\kappa}\\ &= \hbar\sum_{ij}\int\int k_z(\boldsymbol{\kappa})F_i^*(\boldsymbol{\kappa})F_j(\boldsymbol{\kappa})\,\langle\Psi(z)|\hat{a}_i^\dagger\hat{a}_j|\Psi(z)\rangle d^2\boldsymbol{\kappa}\\ &= \frac{N\hbar}{2}\left(\langle k_z\rangle_p + \langle k_z\rangle_{p'}\right),\end{aligned} \tag{S25}$$

where we used

$$\left(\langle N|_{0p} - \langle N|_{0p'}\right)\sum_{ij}\hat{a}_i^\dagger\hat{a}_j\left(|N\rangle_{0p} - |N\rangle_{0p'}\right) = N\delta_{ip}\delta_{jp} + N\delta_{ip'}\delta_{jp'}\,, \tag{S26}$$

and

$$\langle k_z\rangle_p = \int\int k_z(\boldsymbol{\kappa})F_p^*(\boldsymbol{\kappa})F_p(\boldsymbol{\kappa})d^2\boldsymbol{\kappa}\,, \tag{S27}$$

is the classical average of the longitudinal wave vector k_z for the mode p. Similarly, we obtain that

$$\langle\Psi(z)|\hat{P}_z^2|\Psi(z)\rangle = \frac{\hbar^2}{2}\left[(N^2-N)\left(\langle k_z\rangle_p^2+\langle k_z\rangle_{p'}^2\right)+N\left(\langle k_z^2\rangle_p+\langle k_z^2\rangle_{p'}\right)\right]. \tag{S28}$$

The resulting QFI is, therefore

$$F_Q(|\Psi(z)\rangle) = 4\frac{\Delta^2\hat{P}_z\big|_\Psi}{\hbar^2} = 2N\left(\Delta^2 k_z|_p+\Delta^2 k_z|_{p'}\right)+N^2\left(\langle k_z\rangle_p-\langle k_z\rangle_{p'}\right)^2, \tag{S29}$$

where $\Delta^2 k_z\big|_p = \langle k_z^2\rangle - \langle k_z\rangle^2$, and equivalently for p'.

To obtain further insight on the QFI, we swap the modes p and p' to the Hermite-Gaussian (HG) modes HG_{mn} and $\mathrm{HG}_{m'n'}$, respectively. In the HG basis, the average and variance of the longitudinal wave vector have the simple expressions

$$\Delta^2 k_z|_p = \frac{1}{8z_r^2}\left[S_2+S+2\right], \qquad \langle k_z\rangle_p = k-\frac{1}{2z_r}(S+1), \tag{S30}$$

resulting in

$$F_Q(|\Psi(z)\rangle) = \frac{N}{4z_R^2}\left[S_2+S_2'+S+S'+4\right]+\frac{N^2}{4}\left(\frac{d}{dz}\Delta\Phi_G\Big|_{z=0}\right)^2, \tag{S31}$$

where $S=m+n$ is the mode order, $S_2=m^2+n^2$ (with equivalent expressions for S' and S_2'), and $\Delta\Phi_G(z)=(S-S')\tan^{-1}(z/z_r)$ is the Gouy phase difference between the modes. The QFI is z-independent, consistent with the self-similarity of the angular spectrum upon propagation. It is worth noting that the second term of the QFI remains unaltered in the LG basis, while a closed form for the first term can be obtained by decomposing the LG modes in the HG basis [10].

We note that the QFI is comprised of two fundamentally distinct terms. The first, standard-quantum limited (proportional to N), increases monotonically with the indices of the modes p and p', and thus with dimension of the state space. We hypothesize that this term carries information about the full distribution of photons in the transverse plane, such that it's retrieval cannot be fully achieved by interferometric measurements alone. On the other hand, the second term displays Heisenberg-limited scaling (proportional to N^2) and increases with the slope of the Gouy phase difference at the focus

$$\frac{d}{dz}\Delta\Phi_G\Big|_{z=0} = \frac{(S-S')}{z_r}. \tag{S32}$$

Equation (S31), therefore, suggests that measurements of the quantum Gouy phase with N00N states can reach quantum-optimal sensitivity in the estimation of longitudinal displacements.

To support our claim, we also calculate the classical Fisher information using the modeled measurement probability (S16) without the wavefront curvature. Assuming $|A_p| = |A_{p'}| = A$ independent of z, around the region of interest $z = 0$, we obtain [11]

$$\begin{aligned} F(z) &= \sum_{i=1,2} \frac{1}{P_i} \left| \frac{\partial P_i}{\partial z} \right|^2 , \\ &= F_Q[\mathcal{O}(N^2)] \left[\frac{4P_{max} \cos^2 \left(N\delta p \tan^{-1}(z/z_R) \right)}{1 - P_{max} \sin^2 \left(N\delta p \tan^{-1}(z/z_R) \right)} \right] , \end{aligned} \tag{S33}$$

where $P_{max} = 2A^{2N}$, $F_Q[\mathcal{O}(N^2)]$ is the QFI term proportional to N^2, P_1 is given by (S16) and $P_2 = 1 - P_1$. The maximum value of the Fisher information is obtained at the focus, and it's given by

$$F(0) = 4P_{max} F_Q[\mathcal{O}(N^2)] . \tag{S34}$$

The above equation shows that the proposed measurement setup is indeed sensitive to the Heisenberg-limited part of the QFI, but does not capture any of the information contained in the SQL part. It is worth noting that equations (S33) and (S34) are valid in the limit where the SMF mode is much smaller than the input modes, such that the contribution from the wavefront curvature to the measurement probability is negligible. In this case, the high losses yield $A \ll 1$ and the Fisher information is far from reaching its quantum bound.

5 Experimental details

The experimental setup consists of a photon pair source and the spatial mode manipulation part (see Fig. S1 for a detailed schematic). In the photon pair source we use a 405 nm continuous-wave pump laser focused down to a 12 mm long, periodically poled nonlinear crystal made out of potassium titanyl phosphate (ppKTP). The pump laser had a slightly astigmatic focus with an approximately 67 μm Gaussian beam waist, in air, at the crystal position. In the crystal, some of the 405 nm photons go through spontaneous parametric downconversion (SPDC) which is type 0 phase matched. The frequencies of the two emerging 810 nm photons were made degenerate by tuning the phase matching by controlling the temperature of the crystal. After the SPDC, the pump laser is filtered out using two bandpass filters (BPF), where the first one has a 10 nm bandpass and the second one a 3 nm bandpass around 810 nm. The first filter is used to remove the pump laser and the second filter is used to tune the spectral properties of the photon pair. To split each pair of photons, we use their momentum anti-correlations by placing a lens one

focal length away from the crystal after which we place a D-shaped mirror one focal length behind the lens. The lens then performs an optical Fourier transform and the momentum anti-correlations of the photons are used to split each pair. After splitting the photons, one of them is sent through a delay stage which controls the temporal indistinguishability of the two photons. The photons are then coupled into separate SMF's placed on coupling stages (xyz) using a lens and a microscope objective.

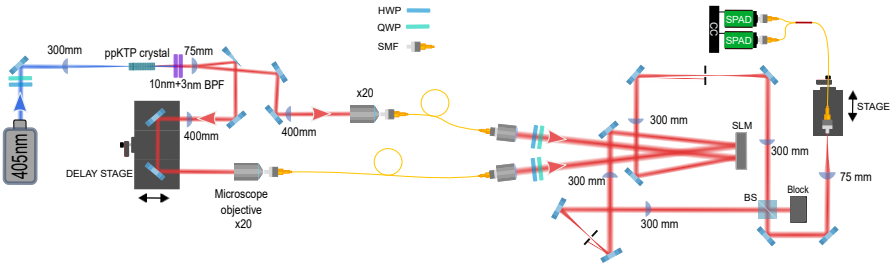

Fig. S1 A detailed drawing of the experimental system. The photon pair source (left) generates photon pairs which are split and coupled into SMF's. The source also includes a delay stage which can tune the temporal distinguishability of the photon pair. The photons are sent to the spatial mode manipulation setup using the SMF's after which they are sent onto two separate regions of a spatial light modulator (SLM). After the photons have been strucutred at the SLM they are imaged with 4f systems to roughly one focal length away from the 75 mm lens which is used to focus the photons onto a SMF placed on a stage. Within these identical 4f systems we place a beamsplitter (BS) which is used to probabilistically combine the photons into the same beam path. The half wave plates (HWP) and quarter wave plates (QWP) are used to facilitate optimum efficiency of the polarization dependent SPDC process and the SLM.

The photons then exit the SMF's after which they are collimated and sent through waveplates which align their polarizations such that the polarization sensitive SLM operates at optimum efficiency. The SLM used was a Holoeye Pluto 2 and it was wavefront corrected using the method described in [12]. The two photons are then modulated on two separate regions of the SLM, using mode carving which is a technique where amplitude and phase modulation can be performed on a single phase-only hologram [13]. In the process, a transverse field structure $|u_A(x,y)|e^{-\mathrm{i}\Phi(x,y)}$ is carved onto the first diffraction order of the hologram, out of a larger Gaussian input beam. Quite often the effects of the initial Gaussian structure of the input beam are removed by making the Gaussian large enough to have an effectively flat amplitude distribution in the area of the hologram. However, to produce the best possible modes at the beam radius required for our measurements, we removed the structure of the initial Gaussian by generating a hologram for the field $\frac{|u_A(x,y)|}{u_0(x,y;\,w_{\mathrm{in}})}e^{-\mathrm{i}\Phi(x,y)}$ using the same mode carving technique. This effectively removes the structure of the incident Gaussian $u_0(x,y;\,w_{\mathrm{in}})$ in the first diffraction order, and we only need to measure the radius w_{in} of the beam

and do not have to worry about making the incident Gaussian much larger than the hologram. However, we note that the incident Gaussian still needs to be slightly larger than the hologram for optimal performance. For more information on this added Gaussian correction see the supplementary of [14].

At the SLM, we structure one of the photons in the p-mode superposition $\frac{1}{\sqrt{2}}[u_{00}(\boldsymbol{\rho},0) - e^{\mathrm{i}\theta_1}u_{0p'}(\boldsymbol{\rho},0)]$ and the other one in the superposition $\frac{1}{\sqrt{2}}[u_{00}(\boldsymbol{\rho},0) + e^{\mathrm{i}\theta_2}u_{0p'}(\boldsymbol{\rho},0)]$. Here the phases θ_1 and θ_2 correspond to small corrections that need to be made due to slight imperfections in the imaging. Due to these same imperfections, we employed additional lens terms on one of the holograms to match the focal points of the two beams as closely as possible. After structuring, both photons go into identical 4f imaging systems and they are also sent into the same beam path, probabilistically, using a 50:50 beamsplitter. Once in the same beam path the photons can bunch into the radial mode N00N state, as long as they are indistinguishable in every degree of freedom, which we verified in our experiments as shown below. After this, the photons are focused down using a 75 mm focusing lens on to a SMF (Thorlabs 780HP FC/PC) placed on a translation stage that scans the SMF through the focus using a computer controlled piezo actuator (Thorlabs PIA13). The final SMF is placed on a coupling stage (xyz) connected to a mount which can control the tip and tilt of the SMF. After the photons are coupled into the SMF, we split them using a 50:50 fiber beamsplitter and sent them into separate single-photon avalanche diodes (SPAD; laser components COUNT T) from which we post-selected on coincident detections of two photons using a coincidence counter (CC; IDQ ID900). The accidental coincidences were removed from all of the data. We calculated the accidental rates as $R_1R_2\tau$, when R_i correspond to the measured single photon rates in each detector and $\tau = 1$ ns is the coincidence window used.

In the measurements we initially set the stage as far away from the focus as possible and moved it closer to the lens, scanning the focus in discrete steps. When calculating the distance between subsequent measurement points, we used the typical step size provided for the piezo actuator (20 nm per piezo step). However, the manufacturer states that this step size can vary up to 20 % depending on the component variance, change of direction, and application conditions. Thus we tried to keep the conditions of the lab consistent while only scanning the piezo in one direction for all of the measurement.

For the measurements with a laser, an 810 nm continuous-wave laser was used and we only required one input hologram. We also replaced the coincident detection scheme with a power meter before and after the setup. The results were then calculated as the power measured after the last SMF normalized by the power measured before the laser was coupled out of the input SMF. The reference power was measured continuously by splitting the input light field using a fiber beamsplitter. Additionally, when structuring the laser field into the superposition $\frac{1}{\sqrt{2}}[u_{00}(\boldsymbol{\rho},0) - u_{0p'}(\boldsymbol{\rho},0)]$ at the measurement fiber, we had to take into account the differing Gouy phases of odd and even order modes. Hence, when p was an odd integer we had to generate

the field $\frac{1}{\sqrt{2}}[u_{00}(\boldsymbol{\rho},0) + e^{\mathrm{i}\theta_1}u_{0p'}(\boldsymbol{\rho},0)]$ instead of $\frac{1}{\sqrt{2}}[u_{00}(\boldsymbol{\rho},0) - e^{\mathrm{i}\theta_1}u_{0p'}(\boldsymbol{\rho},0)]$ to compensate for the π phase difference in Gouy phase when performing the optical Fourier transform of the field.

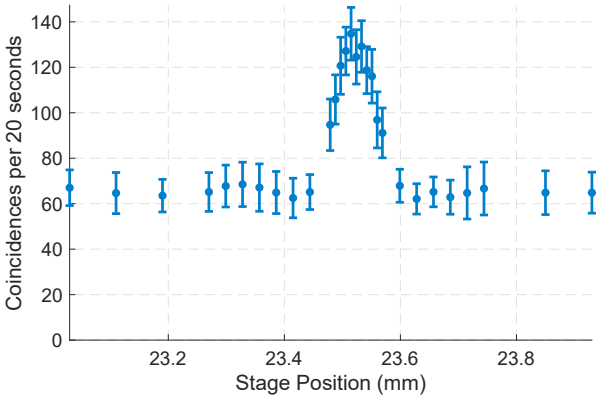

Fig. S2 Measured photon bunching curve with two photons in orthogonal radial mode superpositions. Accidental coincidences have been removed from the data and the errorbars (mean ± standard deviations) are calculated from 21 repetitions of the measurement. The change in stage position should be multiplied by two to arrive at the effective path length change (see Fig. S1 for the configuration of the mirrors on the delay stage). The results show that the rate at which the photon pairs couple into the SMF roughly doubles when the photons bunch into a radial mode N00N state.

To verify photon bunching in to radial mode N00N states, we set the final SMF close to the focus of the field and generated a radial mode N00N state $\frac{1}{\sqrt{2}}[|2,0\rangle_{0,2} + |0,2\rangle_{0,2}]$ by individually structuring the photons into the superpositions $\frac{1}{\sqrt{2}}[u_{00}(\boldsymbol{\rho},0) - \mathrm{i}u_{02}(\boldsymbol{\rho},0)]$ and $\frac{1}{\sqrt{2}}[u_{00}(\boldsymbol{\rho},0) + \mathrm{i}u_{02}(\boldsymbol{\rho},0)]$, as described earlier. We then scan the delay stage in the source to vary the distinguishability of the photons. From the results of the scan (Fig. S2) we see that, as expected, the rate of photon pairs coupling into the SMF roughly doubles when the photons are made indistinguishable.

References

[1] Torres, J.P., Deyanova, Y., Torner, L., Molina-Terriza, G.: Preparation of engineered two-photon entangled states for multidimensional quantum information. Physical Review A **67**(5), 052313 (2003). https://doi.org/10.1103/PhysRevA.67.052313

[2] Wünsche, A.: Quantization of Gauss–Hermite and Gauss–Laguerre beams in free space. Journal of Optics B: Quantum and Semiclassical Optics **6**(3), 47 (2004)

[3] Baladron-Zorita, O., Wang, Z., Hellmann, C., Wyrowski, F.: Isolating the Gouy phase shift in a full physical-optics solution to the propagation problem. JOSA A **36**(9), 1551–1558 (2019). https://doi.org/10.1364/JOSAA.36.001551

[4] Saleh, B.E.A., Teich, M.C.: Fundamentals of Photonics. John Wiley & sons, (1991). Chap. 4.1-4.2

[5] Andrews, D.L., Babiker, M.: The Angular Momentum of Light. Cambridge University Press, (2012)

[6] Kawase, D., Miyamoto, Y., Takeda, M., Sasaki, K., Takeuchi, S.: Observing quantum correlation of photons in Laguerre-Gauss modes using the Gouy phase. Physical review letters **101**(5), 050501 (2008). https://doi.org/10.1103/PhysRevLett.101.050501

[7] Giovannetti, V., Lloyd, S., Maccone, L.: Advances in quantum metrology. Nature photonics **5**(4), 222–229 (2011). https://doi.org/10.1038/nphoton.2011.35

[8] Demkowicz-Dobrzański, R., Jarzyna, M., Kołodyński, J.: Quantum limits in optical interferometry. Progress in Optics **60**, 345–435 (2015). https://doi.org/10.1016/bs.po.2015.02.003

[9] Barbieri, M.: Optical Quantum Metrology. PRX Quantum **3**(1), 010202 (2022). https://doi.org/10.1103/PRXQuantum.3.010202

[10] Beijersbergen, M.W., Allen, L., Van der Veen, H.E.L.O., Woerdman, J.: Astigmatic laser mode converters and transfer of orbital angular momentum. Optics Communications **96**(1-3), 123–132 (1993). https://doi.org/10.1016/0030-4018(93)90535-D

[11] Polino, E., Valeri, M., Spagnolo, N., Sciarrino, F.: Photonic quantum metrology. AVS Quantum Science **2**(2), 024703 (2020). https://doi.org/10.1116/5.0007577

[12] Jesacher, A., Schwaighofer, A., Fürhapter, S., Maurer, C., Bernet, S., Ritsch-Marte, M.: Wavefront correction of spatial light modulators using an optical vortex image. Optics express **15**(9), 5801–5808 (2007). https://doi.org/10.1364/OE.15.005801

[13] Bolduc, E., Bent, N., Santamato, E., Karimi, E., Boyd, R.W.: Exact solution to simultaneous intensity and phase encryption with a single

phase-only hologram. Optics letters **38**(18), 3546–3549 (2013). https://doi.org/10.1364/OL.38.003546

[14] Plachta, S.Z.D., Hiekkamäki, M., Yakaryılmaz, A., Fickler, R.: Quantum advantage using high-dimensional twisted photons as quantum finite automata. Quantum **6**, 752 (2022). https://doi.org/10.22331/q-2022-06-30-752